SUPPLEMENTAL MATERIALS

How Structural and Vibrational Features Affect Optoelectronic Properties of Non-Stoichiometric Quantum Dots: Computational Insights

Manav Bhati,[a,b,c] Sergei A. Ivanov,[d,e] Thomas P. Senftle,[c] Sergei Tretiak,[a,b,e,*]

Dibyajyoti Ghosh [a,b,e,f*]

[a] *Theoretical Division, Los Alamos National Laboratory, Los Alamos, NM, 87545, USA*

[b] *Center for Nonlinear Studies, Los Alamos National Laboratory, Los Alamos, NM, 87545, USA*

[c] *Department of Chemical and Biomolecular Engineering, Rice University, 6100 Main Street, Houston, TX 77005-1892, USA*

[d] *Materials Physics and Applications Division, Los Alamos National Laboratory, Los Alamos, New Mexico, 87545 USA*

[e] *Center for Integrated Nanotechnologies, Los Alamos National Laboratory, Los Alamos, NM, 87545, USA*

[f] *Department of Materials Science and Engineering and Department of Chemistry, Indian Institute of Technology, Delhi, Hauz Khas, New Delhi 110016, India*

[*] Corresponding authors; E-mails: serg@lanl.gov, dibyajyoti@iitd.ac.in

Computational Methodology

All the QD structures employed in this work have been derived from our previous work on investigating static non-stoichiometric QDs, where the structures were optimized to their ground-states.[1] The initial (unoptimized) structures had T_d symmetry with a hybrid wurtzite/zinc-blende arrangement of Cd and Se atoms, where wurtzite arrangement was present on the vertices of the tetrahedron, and zinc-blende arrangement was present in the core of the tetrahedron. Here, we utilized *ab-initio* molecular dynamics (AIMD) simulations based on density functional theory (DFT) to run the dynamical simulations of QDs. The simulations were performed using the Vienna *ab-initio* simulation package (VASP 5.4.4)[2,3] with a plane-wave basis set. The Perdew-Burke-Ernzerhof (PBE)[4] generalized gradient approximation (GGA) for the exchange-correlation functional was used with the projector augmented wave (PAW)[5] potentials. The core electrons were considered frozen and the valence electrons of Se-$4s^2 4p^4$, Cd-$4d^{10} 5s^2$, H-$1s^1$, and Cl-$3s^2 3p^5$ were treated self-consistently. The energy cutoff of 400 eV was used for truncating the plane-wave

basis set and a Monkhorst-Pack (MP)[6] k-point mesh of 1×1×1 was employed to sample the Brillouin zone. Grimme's DFT-D3 dispersion correction[7] was applied to account for van-der-Waals interactions.

The QDs were placed in a 30Å×30Å×30Å simulation cell, such that the periodic images were separated by at least 15Å and did not have any spurious interactions. The ground state QD structures were first heated from 0 K to 300 K using repeated velocity rescaling for 3 ps. Then these structures were equilibrated at 300 K again using velocity rescaling for another 6 ps. Finally, the structures were equilibrated in a microcanonical NVE ensemble for 35 ps. The first 25 ps of this final step were considered equilibration and the final 10 ps were considered as the production-run to be utilized for the analysis of various properties. For the integration of Newton's equations of motions in the AIMD simulations, we chose a timestep of 1 fs. As our main aim in this work is to understand the thermal effects on dynamics of QDs, we have performed the AIMD simulations in gas phase, without considering the solvation effects. This choice is well justified by the amount of dynamical trajectory that we have been able to capture (at picosecond timescales), which otherwise would have been very challenging using dynamical solvation in VASP computational package. Future work will aim at addressing the effects of solvation on the dynamics.

For quantifying the influence of thermal effects on the structure of the QDs, root-mean square fluctuations (RMSF) of both Cd and Se atoms were determined. The RMSF is evaluated by measuring how much each atom fluctuated from its mean position during the MD production simulation. This provides an average fluctuation for each atom over the simulation and the root mean square is evaluated considering all atoms of the same kind (Cd or Se). This calculation involves aligning the coordinates of all the atoms so that only the fluctuations of atoms could be measured excluding the effects of translation and rotation of QD. This alignment and RMSF calculations were performed in the visual molecular dynamics (VMD) software.[8] The power spectra were obtained from the AIMD trajectory by calculating the Fourier transform of the velocity autocorrelation function of the QD atoms. An open-access code, Trajectory Analyzer and Visualizer (TRAVIS)[9–12] was utilized to obtain these power spectra. The off-resonant Raman spectra were obtained from DFT calculations using Gaussian16[13] software package, where the B3LYP[14,15] hybrid exchange-correlational functional was used. Here the atom-centered basis sets were used: LANL2DZ[16–18] for Cd and Se (effective core potential (ECP) LANL2 was used for

core electrons with the double-zeta quality treatment of valence electrons), and full electron 6-31G*[19,20] basis set was used for H and Cl atoms. The geometry optimization was first performed followed by the frequency analysis, which yielded off-resonant Raman Spectra. A Gaussian broadening with a half-width at half-height of 4 cm^{-1} was employed to obtain the Raman spectra from the calculated line-stick spectra. The frequencies from the peaks of the Raman spectra in the optical region were visualized using the Chemcraft software.[21] Note that, Frohlich mechanism that captures the interaction between longitudinal optical phonon modes and electrons, is not explicitly included in these calculations. We verified that Raman spectra do not change with larger basis sets. As shown in **Figure S5**, the spectra calculated for Se-rich QD, using triple-split CEP-121G,[22–24] Stuttgart SDD[25] bases (with and without polarization) appear similar to the one calculated using LANL2DZ basis. For the polarization in SDD, one d and one f polarization functions are added on Se and Cd, respectively. The exponents for the polarization functions are 0.338 and 1.598, respectively, taken from Def2-SVP basis set.[26] In addition, the peaks of the spectra represent similar vibrational modes.

For the electronic structure calculations, the structures were sampled every 20 fs of the AIMD simulation, corresponding to a total of 500 structures for each simulation. The HOMO and LUMO were visualized using the VESTA[27] v3.5.7 software package. The NAMD simulations were performed using the first 5 ps AIMD production-run trajectories. For each QD, 5000 structures from the AIMD trajectory and 500 stochastic realizations were considered for calculating the electron-hole pair recombination over a period of 20 ps using the PYXAID code.[28,29] This code employs the neglect of back-relaxation approximation (NBRA), where it is assumed that the change in the electronic state does not affect the nuclear trajectories. This approach is based on the classical path approximation (CPA). We believe that this approximation is appropriate for the current study as we model small charge-neutral QDs, ligated with strongly bound ligands, not undergoing ligand loss with subsequent creation of surface defects or severe surface modifications during electronic excitations. The population dynamics with time has been calculated using density matrix formalism.[23] Due to the lack of detailed theoretical formalism, the excitonic effects have not been considered in the present NAMD simulations. The vibrationally-induced dephasing processes and associated timescales are calculated using the optical response function formalism. [23] We note that the choice of functionals affect the quantitative results from NAMD simulations,

however, employing hybrid functionals or considering many-body effects requires significant computational effort and could be explored as a separate study.

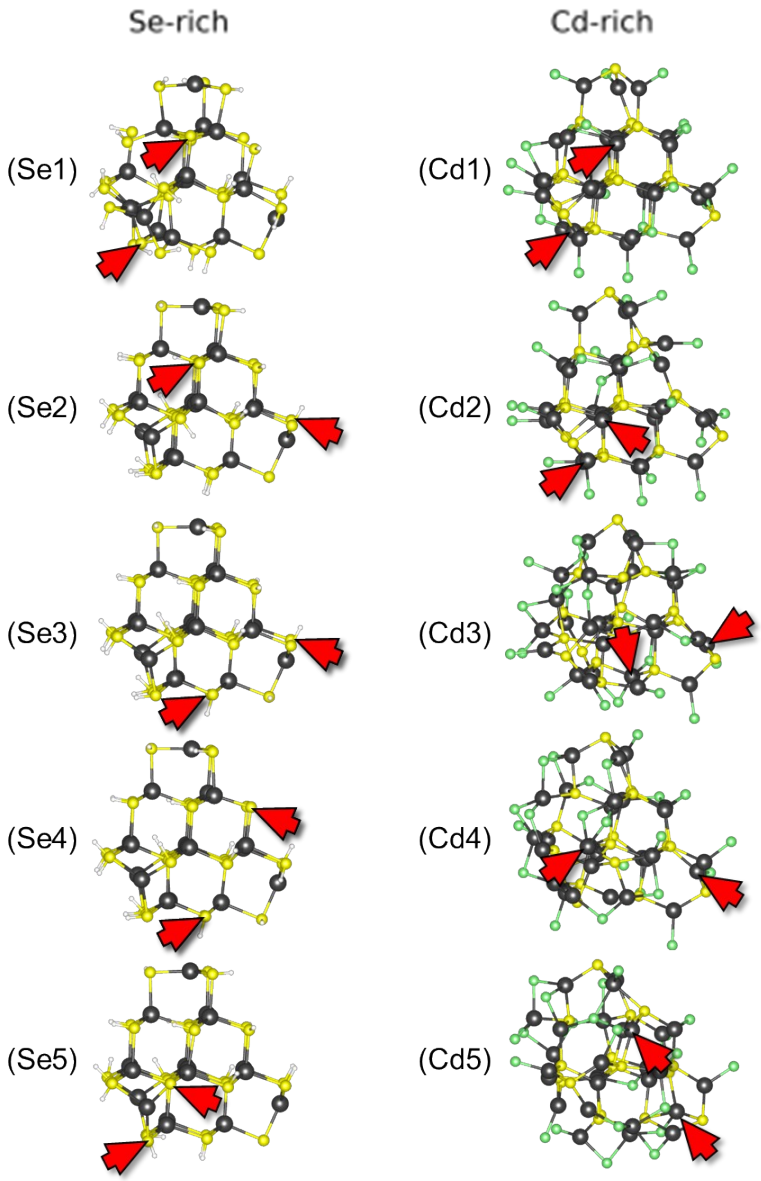

Figure S1. The ground state atomic structures of the five QD configurations for Se-rich and Cd-rich QDs, derived from our previous work.[1] The red arrows point to the surface atoms that are non-ligated (without ligand capping) before geometry optimization. Atoms in yellow: Se, grey: Cd, white: H, green: Cl.

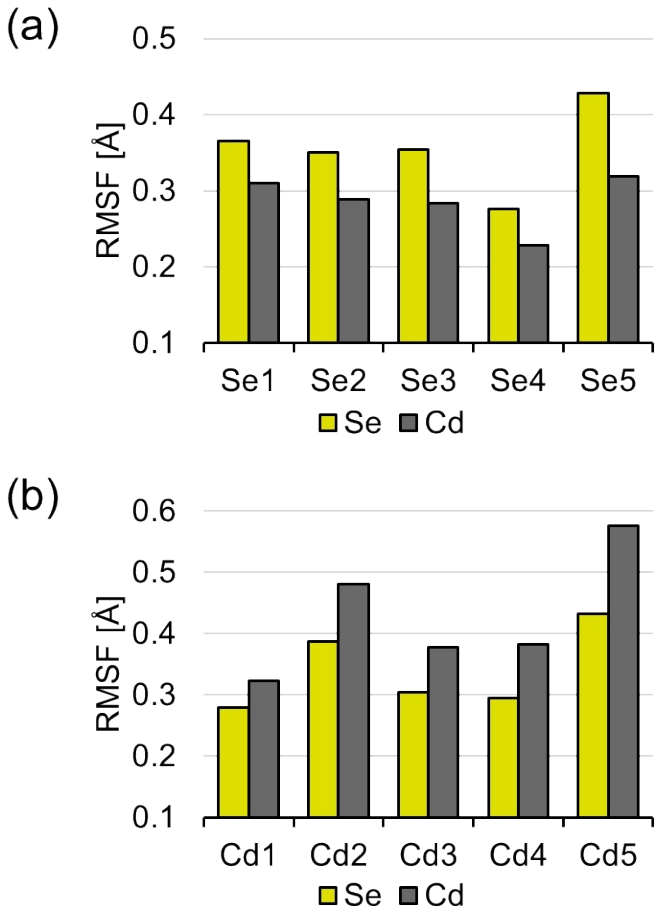

Figure S2. The root-mean-square fluctuation (RMSF) of Se and Cd atoms in five configurations of (a) Se-rich and (b) Cd-rich QDs. The RMSF values for each configuration are derived from the last 10 ps of the AIMD simulations at 300 K. The indexing of QDs corresponds to their energetic stability at room temperature, where the configurations are numbered in the ascending order of energy, i.e. Se1 is more energetically stable compared to Se5. Se atoms in all Se-rich QDs have higher fluctuations compared to Cd atoms, whereas Cd atoms in all Cd-rich QDs have higher fluctuations compared to Se atoms.

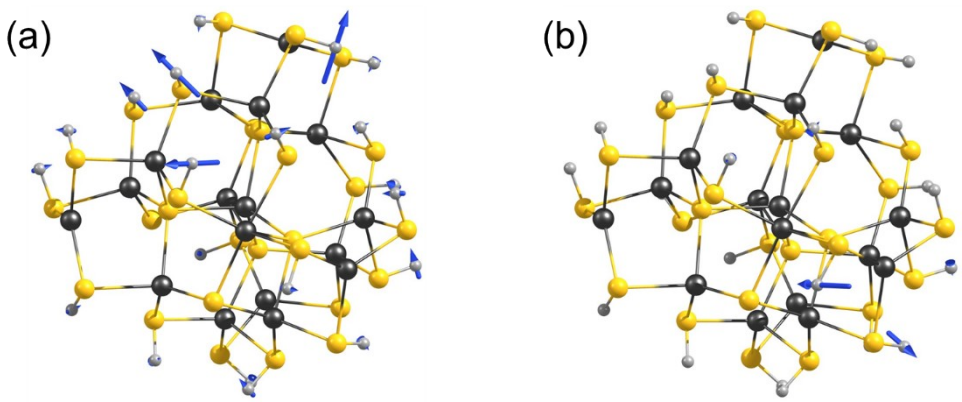

Figure S3. The representative vibrational modes corresponding to the peaks in the frequency range above 300 cm^{-1} in the Raman spectrum of Se-rich QD. The plotted modes appear at (a) 405 cm^{-1} and (b) 432 cm^{-1}. These high frequency modes originate from the Se-H bending. The blue arrows reflect the displacement vectors of respective atoms.

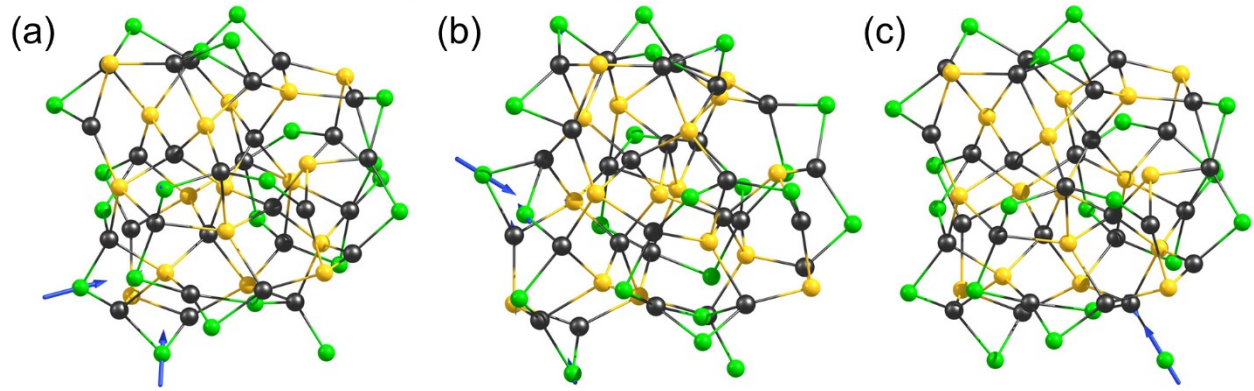

Figure S4. The representative vibrational modes corresponding to the peaks in the frequency range above 220 cm^{-1} in the Raman spectrum of Cd-rich QD. The plotted modes correspond to peaks at (a) 237 cm^{-1}, (b) 253 cm^{-1}, and (c) 311 cm^{-1}. These high frequency modes originate from the Cd-$Cl_{(terminal)}$ stretching motion. The blue arrows reflect the displacement vectors of respective atoms.

Note that the distinct sharp peak at 311 cm^{-1} for this QD is assigned to the stretching mode of a Cd-Cl bond on the surface (Supplemental Figure S4). Such peak most likely appears due to a coincidentally specific configuration of atoms on the modeled surface and cannot be considered as the general vibrational feature.

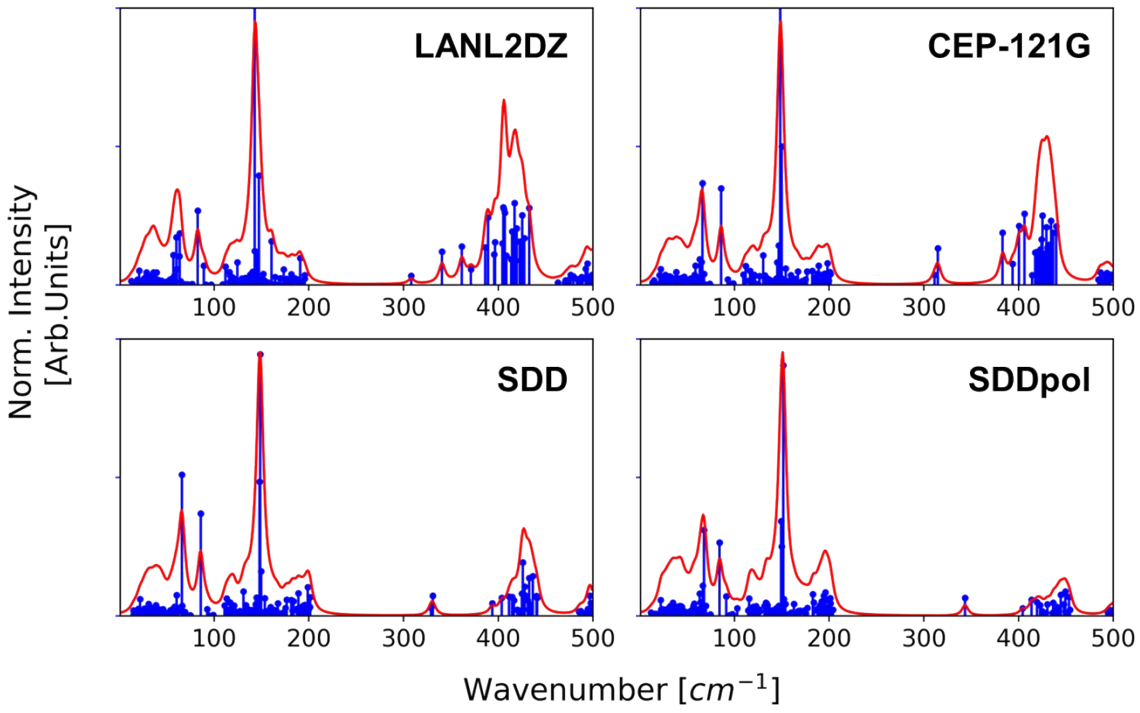

Figure S5. Raman Spectra calculated for Se-rich QD using four basis sets: LANL2DZ, CEP-121G, SDD, and SDD with polarization (SDDpol). The spectra (shown in red) are obtained with Gaussian broadening (half-wide at half-height of 4 cm^{-1}) of the line-stick spectra (shown in blue) defining the positions of the vibrational normal modes and their Raman intensities.

References

(1) Bhati, M.; Ivanov, S. A.; Senftle, T. P.; Tretiak, S.; Ghosh, D. Nature of Electronic Excitations in Small Non-Stoichiometric Quantum Dots. *J. Mater. Chem. A* **2022**, *10* (10), 5212–5220. https://doi.org/10.1039/D1TA07983B.

(2) Kresse, G.; Furthmüller, J. Efficient Iterative Schemes for Ab Initio Total-Energy Calculations Using a Plane-Wave Basis Set. *Phys. Rev. B* **1996**, *54* (16), 11169–11186. https://doi.org/10.1103/PhysRevB.54.11169.

(3) Kresse, G.; Furthmüller, J. Efficiency of Ab-Initio Total Energy Calculations for Metals and Semiconductors Using a Plane-Wave Basis Set. *Computational Materials Science* **1996**, *6* (1), 15–50. https://doi.org/10.1016/0927-0256(96)00008-0.

(4) Perdew, J. P.; Burke, K.; Ernzerhof, M. Generalized Gradient Approximation Made Simple. *Phys. Rev. Lett.* **1996**, *77* (18), 3865–3868. https://doi.org/10.1103/PhysRevLett.77.3865.

(5) Kresse, G.; Joubert, D. From Ultrasoft Pseudopotentials to the Projector Augmented-Wave Method. *Phys. Rev. B* **1999**, *59* (3), 1758–1775. https://doi.org/10.1103/PhysRevB.59.1758.

(6) Monkhorst, H. J.; Pack, J. D. Special Points for Brillouin-Zone Integrations. *Phys. Rev. B* **1976**, *13* (12), 5188–5192. https://doi.org/10.1103/PhysRevB.13.5188.

(7) Grimme, S.; Antony, J.; Ehrlich, S.; Krieg, H. A Consistent and Accurate Ab Initio Parametrization of Density Functional Dispersion Correction (DFT-D) for the 94 Elements H-Pu. *J. Chem. Phys.* **2010**, *132* (15), 154104. https://doi.org/10.1063/1.3382344.

(8) Humphrey, W.; Dalke, A.; Schulten, K. VMD: Visual Molecular Dynamics. *Journal of Molecular Graphics* **1996**, *14* (1), 33–38. https://doi.org/10.1016/0263-7855(96)00018-5.

(9) Brehm, M.; Thomas, M.; Gehrke, S.; Kirchner, B. TRAVIS—A Free Analyzer for Trajectories from Molecular Simulation. *J. Chem. Phys.* **2020**, *152* (16), 164105. https://doi.org/10.1063/5.0005078.

(10) Brehm, M.; Kirchner, B. TRAVIS - A Free Analyzer and Visualizer for Monte Carlo and Molecular Dynamics Trajectories. *J. Chem. Inf. Model.* **2011**, *51* (8), 2007–2023. https://doi.org/10.1021/ci200217w.

(11) Thomas, M.; Brehm, M.; Fligg, R.; Vöhringer, P.; Kirchner, B. Computing Vibrational Spectra from Ab Initio Molecular Dynamics. *Phys. Chem. Chem. Phys.* **2013**, *15* (18), 6608–6622. https://doi.org/10.1039/C3CP44302G.

(12) Thomas, M.; Brehm, M.; Kirchner, B. Voronoi Dipole Moments for the Simulation of Bulk Phase Vibrational Spectra. *Phys. Chem. Chem. Phys.* **2015**, *17* (5), 3207–3213. https://doi.org/10.1039/C4CP05272B.

(13) Frisch, M. J.; Trucks, G. W.; Schlegel, H. B.; Scuseria, G. E.; Robb, M. A.; Cheeseman, J. R.; Scalmani, G.; Barone, V.; Petersson, G. A.; Nakatsuji, H.; et al. Gaussian 16, Revision A.03, 2016.

(14) Becke, A. D. Density-functional Thermochemistry. III. The Role of Exact Exchange. *J. Chem. Phys.* **1993**, *98* (7), 5648–5652. https://doi.org/10.1063/1.464913.

(15) Lee, C.; Yang, W.; Parr, R. G. Development of the Colle-Salvetti Correlation-Energy Formula into a Functional of the Electron Density. *Phys. Rev. B* **1988**, *37* (2), 785–789. https://doi.org/10.1103/PhysRevB.37.785.

(16) Ditchfield, R.; Hehre, W. J.; Pople, J. A. Self-Consistent Molecular-Orbital Methods. IX. An Extended Gaussian-Type Basis for Molecular-Orbital Studies of Organic Molecules. *J. Chem. Phys.* **1971**, *54* (2), 724–728. https://doi.org/10.1063/1.1674902.

(17) Hay, P. J.; Wadt, W. R. Ab Initio Effective Core Potentials for Molecular Calculations. Potentials for the Transition Metal Atoms Sc to Hg. *J. Chem. Phys.* **1985**, *82* (1), 270–283. https://doi.org/10.1063/1.448799.

(18) Wadt, W. R.; Hay, P. J. Ab Initio Effective Core Potentials for Molecular Calculations. Potentials for Main Group Elements Na to Bi. *J. Chem. Phys.* **1985**, *82* (1), 284–298. https://doi.org/10.1063/1.448800.

(19) Petersson, G. A.; Bennett, A.; Tensfeldt, T. G.; Al-Laham, M. A.; Shirley, W. A.; Mantzaris, J. A Complete Basis Set Model Chemistry. I. The Total Energies of Closed-shell Atoms and Hydrides of the First-row Elements. *J. Chem. Phys.* **1988**, *89* (4), 2193–2218. https://doi.org/10.1063/1.455064.

(20) Petersson, G. A.; Al-Laham, M. A. A Complete Basis Set Model Chemistry. II. Open-shell Systems and the Total Energies of the First-row Atoms. *J. Chem. Phys.* **1991**, *94* (9), 6081–6090. https://doi.org/10.1063/1.460447.

(21) Chemcraft - Graphical Software for Visualization of Quantum Chemistry Computations. Https://Www.Chemcraftprog.Com. https://www.chemcraftprog.com (accessed 2022-04-15).

(22) Stevens, W. J.; Basch, H.; Krauss, M. Compact Effective Potentials and Efficient Shared-exponent Basis Sets for the First- and Second-row Atoms. *J. Chem. Phys.* **1984**, *81* (12), 6026–6033. https://doi.org/10.1063/1.447604.

(23) Stevens, W. J.; Krauss, M.; Basch, H.; Jasien, P. G. Relativistic Compact Effective Potentials and Efficient, Shared-Exponent Basis Sets for the Third-, Fourth-, and Fifth-Row Atoms. *Can. J. Chem.* **1992**, *70* (2), 612–630. https://doi.org/10.1139/v92-085.

(24) Cundari, T. R.; Stevens, W. J. Effective Core Potential Methods for the Lanthanides. *J. Chem. Phys.* **1993**, *98* (7), 5555–5565. https://doi.org/10.1063/1.464902.

(25) Dunning, Thom. H.; Hay, P. J. Gaussian Basis Sets for Molecular Calculations. In *Methods of Electronic Structure Theory*; Schaefer, H. F., Ed.; Modern Theoretical Chemistry; Springer US: Boston, MA, 1977; pp 1–27. https://doi.org/10.1007/978-1-4757-0887-5_1.

(26) Weigend, F.; Ahlrichs, R. Balanced Basis Sets of Split Valence, Triple Zeta Valence and Quadruple Zeta Valence Quality for H to Rn: Design and Assessment of Accuracy. *Phys. Chem. Chem. Phys.* **2005**, *7* (18), 3297–3305. https://doi.org/10.1039/B508541A.

(27) Momma, K.; Izumi, F. VESTA 3 for Three-Dimensional Visualization of Crystal, Volumetric and Morphology Data. *J Appl Cryst* **2011**, *44* (6), 1272–1276. https://doi.org/10.1107/S0021889811038970.

(28) Akimov, A. V.; Prezhdo, O. V. The PYXAID Program for Non-Adiabatic Molecular Dynamics in Condensed Matter Systems. *J. Chem. Theory Comput.* **2013**, *9* (11), 4959–4972. https://doi.org/10.1021/ct400641n.

(29) Akimov, A. V.; Prezhdo, O. V. Advanced Capabilities of the PYXAID Program: Integration Schemes, Decoherence Effects, Multiexcitonic States, and Field-Matter Interaction. *J. Chem. Theory Comput.* **2014**, *10* (2), 789–804. https://doi.org/10.1021/ct400934c.